



# Spatially, Spectrally Single-Mode and Mechanically Flexible 3D-Printed Terahertz Transmission Waveguides

Bo Chen , Wei Wei, Jingzhu Shao, Borui Xu, Huan Zhu, Gangyi Xu, and Chongzhao Wu 

**Abstract**—Emerged terahertz transmission waveguides or fibers will enable novel terahertz systems and applications. High-quality output beam profiles, mechanical flexibility and reliability are among the most crucial and challenging characteristics of terahertz transmission waveguides. Here, we design and fabricate the flexible and stretchable transmission waveguides by 3D printing to guide radiation from terahertz (THz) quantum cascade lasers (QCLs) lasing at the frequency of 2.58 THz. Composite silver nanoparticles and polydimethylsiloxane are coated on the inner surface of the 3D-printed polycarbonate/rubber substrate tube. Output beam profiles from the transmission waveguides, which are captured by a room-temperature terahertz camera, demonstrate single-mode spatial intensity distribution. Transmission spectra are measured out from the waveguides and single-mode characteristics of THz QCLs are preserved from threshold to peak bias. More than 300 times of bending and force-strain curves are tested for the 3D-printed flexible terahertz transmission waveguides, the propagation losses exhibit no obvious change, demonstrating a superior mechanical endurance.

**Index Terms**—Terahertz waveguide, terahertz quantum cascade lasers, 3D-printing.

## I. INTRODUCTION

TERAHERTZ (THz) waves have attracted increasing attentions in the field of biomedical applications due to the characteristics of being non-ionizing, non-invasive and sensitive to moisture in biological tissues [1], [2]. What's more, many

Manuscript received October 27, 2021; revised December 7, 2021; accepted December 9, 2021. Date of publication December 15, 2021; date of current version December 31, 2021. This work was supported in part by the National Natural Science Foundation of China under Grants 62105201, 61734006, and 61974151, in part by the Natural Science Foundation of Shanghai under Grant 20ZR1428300, in part by the Shanghai Sailing Program under Grant 19YF1425100, in part by the Shanghai Jiao Tong University under Grant NFTM TMSK-2020-105, in part by the Shanghai Jiao Tong University (Medical-Engineering Funding under Grant YG2019QNA58), and in part by the Science and Technology Commission of Shanghai Municipality under Grant 20DZ2220400. (Corresponding author: Chongzhao Wu.)

Bo Chen, Wei Wei, Jingzhu Shao, Borui Xu, and Chongzhao Wu are with the Center for Biophotonics, Institute of Medical Robotics, Shanghai Jiao Tong University, Shanghai 200240, China, and also with the School of Biomedical Engineering, Shanghai Jiao Tong University, Shanghai 200240, China (e-mail: chenbo042117@sjtu.edu.cn; weiwei30@sjtu.edu.cn; answer000@sjtu.edu.cn; xbr\_sjtu265@sjtu.edu.cn; czwu@sjtu.edu.cn).

Huan Zhu and Gangyi Xu are with the Key Laboratory of Infrared Imaging Materials and Detectors, Shanghai Institute of Technical Physics, Chinese Academy of Sciences, Shanghai 200083, China, and also with the Hangzhou Institute for Advanced Study, University of Chinese Academy of Sciences, Hangzhou 310000, China (e-mail: zhuhanhuan@126.com; gangyi.xu@mail.sitp.ac.cn).

Digital Object Identifier 10.1109/JPHOT.2021.3135659

molecules have strong rotational and vibrational absorption features at THz frequencies, leading to spectroscopic fingerprinting in the THz range [3]. Rapid developments in terahertz technologies, such as sources and detectors, have promoted various applications in sensing [4], [5], non-destructive imaging [6] and spectroscopy [7]. However, water vapor and other gas molecules during transmission process could lead to severe absorptions, which limit the applications of terahertz technology. As important and effective methods to guide and deliver THz radiation, terahertz transmission waveguides or fibers have been emerging technologies, which are able to be utilized in THz imaging, sensing and communication [8], [9]. However, due to the high absorption coefficient of many dielectric materials in the wavelength range of THz radiation, high performance terahertz fibers are challenging. So far, various designs of terahertz transmission waveguides, according to the materials and geometries, including circular metals [10], metal wires [11], planar metals [12], dielectric solid-core [13], porous-core [14] and hollow-core with metallic or dielectric coating [15], hollow core antiresonant structures [16] have been explored.

Terahertz quantum cascade lasers (THz QCLs) are the electrically-pumped semiconductor lasers, which emit terahertz radiation due to intersubband optical transitions in semiconductor superlattices [17]. Currently, lasing frequency of THz QCLs ranges from  $\sim 1$  to 5 THz and THz QCLs are the most powerful solid-state THz sources so far. THz QCLs with various designs and schemes have demonstrated single-mode emission [18], collimated beam [19]–[21], frequency tunability [22], [23], high operating temperature [24] and high output power [25]–[28]. For terahertz transmission waveguides which were able to effectively deliver radiation from THz QCLs, Vitiello *et al.* presented a silver-coated polycarbonate waveguide and a hollow aluminum waveguide coupling with edge-emitting and surface-emitting THz QCLs [29], [30]. Cumis *et al.* investigated the effects of metallic and dielectric inner coatings deposited on the silver film of polycarbonate waveguide [31]. Utilizing THz QCLs as radiating sources as well, Degl'Innocenti *et al.* showed a copper pipe structure [32] and Wallis *et al.* demonstrated hollow cylindrical metallic waveguides using un-annealed, annealed copper and stainless steel [33] to guide THz power and coupling with a PS-metallic waveguide [34]. However, metallic wire or metallic tube-based terahertz waveguides are not suitable for the biomedical applications due to the rigidity and poor biocompatibility. In addition to the hollow

cylindrical terahertz waveguides discussed above, Nazarov *et al.* designed a microstructured polymer waveguide to improve the quality of radiation from THz QCLs [35]. However, the fatigue of micro-structured caused by repeated bending would significantly decrease the transmission performance of terahertz waveguides and the fabrication is much more complicated. A low-cost, flexible, mechanically reliable terahertz transmission waveguide with single-mode transmission will be of great importance for related applications.

3D printing technology has been widely utilized in fabrication because it is simple, effective, low-cost and could greatly improve the freedom of designing various structures and schemes [36]. 3D-printed metal-pipe rectangular waveguides were demonstrated in the frequency range of 500–750 GHz and 750 GHz–1.1 THz [37]. Kagome photonic crystal structure-based THz waveguides fabricated by 3D printing were characterized by using terahertz time-domain spectroscopy (THz-TDS) at the frequency of 0.2–1.0 THz [38]. Terahertz plasmonic waveguides with abrupt out-of-plane bends and continuously varying bends were created via 3D printing and measured by THz-TDS as well [39]. 3D-printed THz Bragg waveguide with defect layers achieved THz resonant surface sensing at 0.1–0.5 THz using  $\alpha$ -lactose monohydrate powder as an analyte [40]. 3D-printed dielectric tube THz waveguide with anti-reflection structure showed a close-to-zero dispersion guidance of THz radiation from 0.2–1.0 THz [41]. However, all the 3D-printed THz waveguides are rigid or fragile after bending and stretching. Therefore, 3D-printed terahertz transmission waveguides, which are flexible and stretchable, are highly desired.

In this work, flexible substrate tubes made of polycarbonate/rubber with a shore-A hardness are fabricated by a multi-material 3D printer. Compared with the shore-D hardness materials, such as polycarbonate, resin and polymers [42], the substrate tubes here are much more flexible to be bent easily with a smaller bending radius, which is very crucial for non-destructive inspection and endoscopy in a narrow space. Composite silver nanoparticles (Ag NPs) and polydimethylsiloxane (PDMS) polymers are coated on the inner surface of substrate tube. Silver has been widely used in terahertz transmission waveguides due to a reflectivity larger than 99% in terahertz band and relatively low cost compared with gold. PDMS has steady dielectric characteristics, low transmission loss in the THz wavelength [43] and serves as the role of smoothing the inner surface of the substrate tube fabricated by 3D printing [44]. Transmission loss and beam profiles of the flexible terahertz waveguides are investigated at the frequency of 2.58 THz, which is the lasing frequency of the THz QCL. The results show that the transmission losses of waveguides with 4 and 2 mm-bore diameters are  $\sim 0.22$  dB/cm and  $\sim 0.46$  dB/cm and bending losses with a  $60^\circ$  bending angle are  $\sim 5.6$  dB and  $\sim 8.8$  dB, respectively. The output beam profiles of the 2 mm-bore diameter waveguides exhibit the single-mode Gaussian-like distribution intensity, while the 4 mm-bore diameter waveguides show a dominant single mode spatial distribution with a slightly split output mode. The 3D-printed flexible terahertz waveguides show superior mechanical endurance. More than 300 times of bending are applied to the waveguides, no obvious change is observed in the propagation

losses and force-strain relations of the 3D-printed terahertz waveguides with different bore diameters are tested. To the best of our knowledge, this is the first time to demonstrate 3D-printed flexible and stretchable terahertz transmission waveguides. Such waveguides fabricated by low-cost and flexibly designed 3D printing technology will play an important role in terahertz sensing, non-destructive inspection and medical diagnosis.

## II. FABRICATION AND EXPERIMENTAL SETUP

The fabrication methods of the 3D-printed flexible terahertz transmission waveguides are shown in Fig. 1. Firstly, ProJet MJP 5600 3D printer was used to fabricate substrate tubes. The material of substrate tubes consists of polycarbonate (PC) and rubber with a shore-A hardness (65-75). The thickness of the substrate tubes is 1 mm, with two bore diameters of 2 mm and 4 mm, and two lengths of 10 cm and 20 cm, respectively. The substrate tubes were then washed by alcohol, deionized (DI) water and dried in an oven. Polydimethylsiloxane (PDMS) were prepared by mixing the pre-polymer base (Sylgard 184 silicone elastomer) and curing agent (Sylgard 184 silicone). The absorption coefficient of PDMS in the THz frequency range would decrease slightly when decreasing the weight ratio of curing agent [45]. However, a lower curing agent concentration may lead to a longer curing time. Thus, the curing agent and PDMS pre-polymer base were mixed with the weight ratio of 1:10 and stirred vigorously for 30 mins. Ag nanoparticles (NPs) were added into the PDMS with various weight ratios and stirred for about 30 mins to get composite PDMS and Ag NPs suspended. Next, Ag NPs in PDMS suspension were dried in a vacuum oven for 45 mins to remove bubbles. Finally, the mixture of Ag NPs and PDMS was injected into the 3D-printed substrate tubes for 10 mins at the flow rate of 10 ml/min and cured at an optimized temperature of  $50^\circ\text{C}$  for 5 hours. The composite coating layer of PDMS and Ag NPs was deposited on the inner sidewall of the flexible 3D-printed terahertz transmission waveguides.

The experimental setup of characterizing the fabricated flexible terahertz transmission waveguides is shown in Fig. 2. THz QCLs with a double-metal master-oscillator power-amplifier (MOPA) architecture [46] served as the terahertz radiative sources and were operated in pulsed operation with 400 ns pulse duration and 100 kHz repetition rate under liquid nitrogen condition. Output beam from THz QCLs was coupled into the transmission waveguide with a 25 mm focal length TPX lens, which was placed at the input end of the waveguide. The input and output lasing signal of the terahertz transmission waveguide were recorded by a Golay cell detector, and the corresponding beam profiles were detected by a two-dimensional terahertz array detector operating at room temperature, realizing a real-time detection of spatial intensity distributions. At the bending condition of the 3D-printed flexible THz transmission waveguide, bending radius of the curvature is 5 cm.

Fig. 3(a) shows light-current-voltage (L-I-V) characteristics of the THz-MOPA-QCL operated at 78 K. The lasing threshold voltage and current is  $\sim 8.7$  V and  $\sim 3.3$  A, respectively and the peak output power is  $\sim 32$  mW at 78 K. The incident terahertz distribution at the input end of the waveguide is shown in the

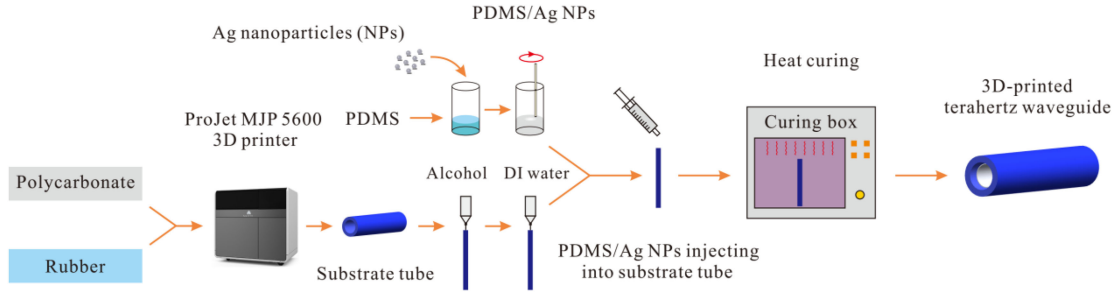


Fig. 1. Schematic of fabrication process for the 3D-printed flexible terahertz transmission waveguide.

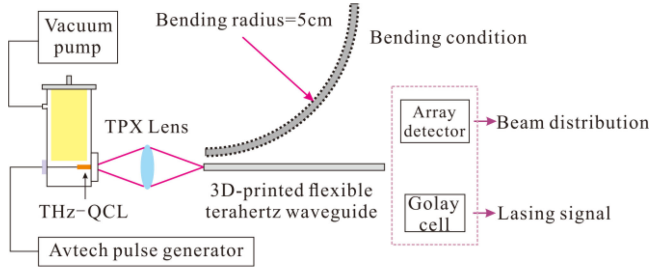


Fig. 2. Schematic of experimental setup to characterize the 3D-printed flexible terahertz transmission waveguides.

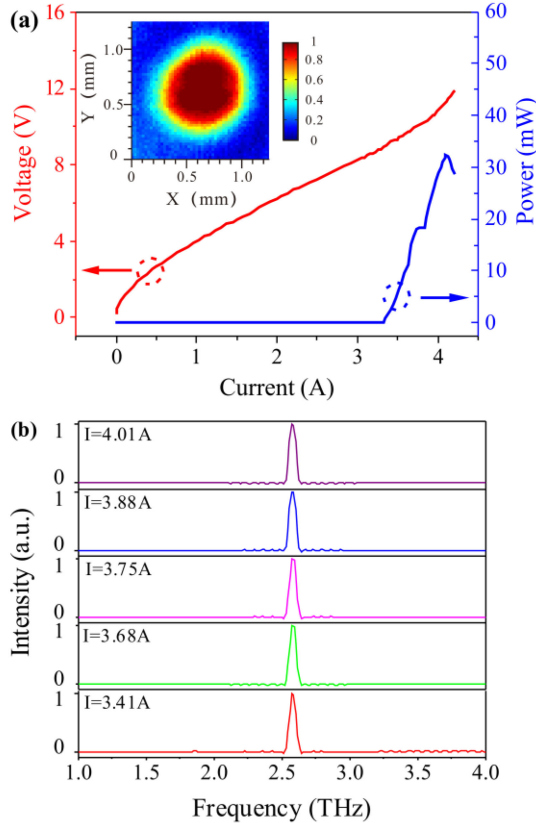


Fig. 3. (a) Experimental light-current-voltage characteristics of the THz QCL at 78 K. The inset shows the beam profile at the entrance of the transmission waveguide and the THz QCL is biased at the current of 3.8 A. (b) Lasing spectra of the THz QCL under different biases from threshold to peak biasing condition.

inset of Fig. 3(a). Lasing frequency of the THz-MOPA-QCL is  $\sim 2.58$  THz and spectra at different biases were recorded by Fourier Transform Infrared Spectrometer (FTIR, Bruker 80V) with a resolution of  $0.5 \text{ cm}^{-1}$  at 78 K in linear-scan mode under vacuum and with a room-temperature DTGS detector placed inside the FTIR. Robust single-mode spectra were measured from the threshold to the peak bias condition of the THz-MOPA-QCL, as shown in Fig. 3(b).

### III. RESULTS AND DISCUSSIONS

PDMS coating layer is not only able to smooth the surface roughness caused by 3D printing accuracy, but also helps adhere the Ag NPs to the inner surface of the 3D printed substrate tubes. Ag NPs form closed and dense structures in PDMS matrix [47] and the composite layer could serve as a reflective layer of the 3D-printed terahertz waveguides. In order to find the optimized number of the composite PDMS and Ag NPs coating layer, the transmission loss of 3D-printed terahertz waveguide was investigated after coating different numbers of layers, as shown in the top scale of Fig. 4(a). Transmission loss of 3D-printed terahertz waveguide was calculated by using Beer-Lambert's law with a cutback method [35]. Due to the high viscosity of the composite PDMS and Ag NPs, which leads to the difficulty of injecting into 3D-printed substrate tube with a 2 mm-bore diameter, the substrate tube with a 4 mm-bore diameter was used as a testing bed. Once introducing one composite PDMS and Ag NPs coating layer, the propagation loss dropped from more than  $0.5 \text{ dB/cm}$  to  $\sim 0.23 \text{ dB/cm}$ , which confirms the functionality of the composite layer to reduce the extra transmission loss and confine THz wave energy in the hollow region of waveguide. Inset of Fig. 4(a) shows the SEM image of the composite PDMS and Ag NPs, indicating the coating layer was deposited successfully on the inner sidewall of substrate tube, with a thickness of  $\sim 100 \mu\text{m}$ . Due to the extra absorption loss induced by PDMS [48], the transmission loss increased to  $\sim 0.35 \text{ dB/cm}$  after depositing three coating layers. Thus, one composite PDMS and Ag NPs coating layer was chosen in the following and further optimization of experimental parameters.

To explore the effect of the composite weight ratio of PDMS and Ag NPs on the propagation loss of waveguides, transmission waveguides with different composite PDMS and Ag NPs weight ratios were fabricated and their transmission loss were characterized. Curing temperature of the composite layer is set as 50

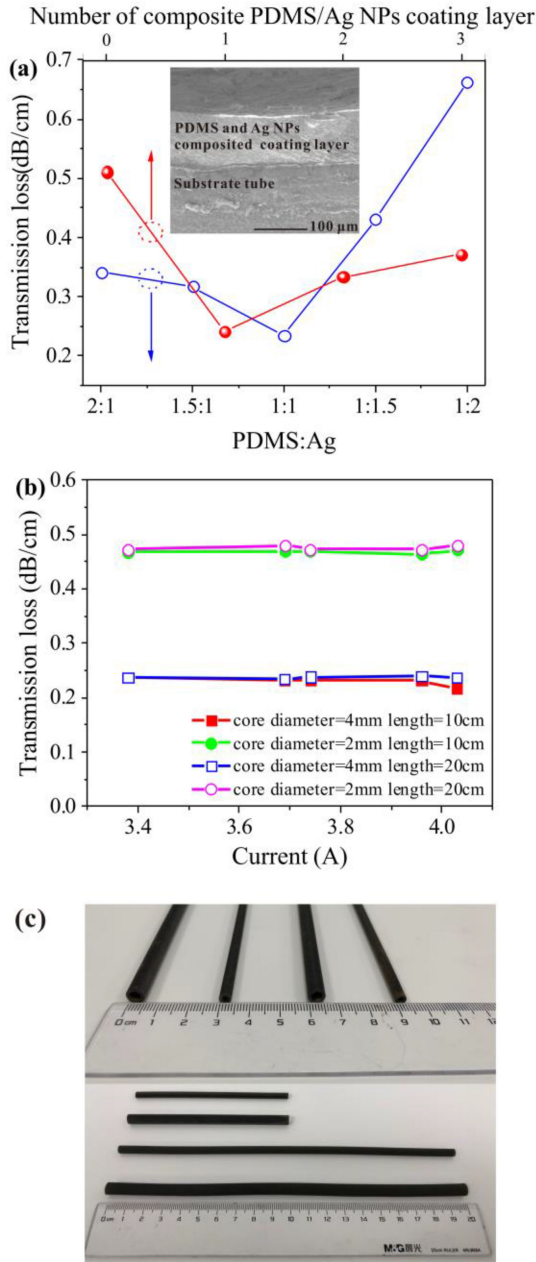


Fig. 4. (a) Transmission loss of the 3D-printed terahertz waveguide with a 4 mm bore diameter versus different PDMS and Ag NPs composite ratios (bottom scale) and different numbers of composite PDMS and Ag NPs coating layer (top scale). The inset shows cross-sectional SEM image of the 3D-printed flexible terahertz waveguide with one PDMS/Ag NPs coating layer. (b) Loss of four terahertz transmission waveguides with 10 cm, 20 cm length and 2 mm, 4 mm bore diameter, respectively at different biases of THz QCL from threshold to peak. (c) Photographs of the four terahertz transmission waveguides with various dimensions shown in (b).

°C by considering both successful curing and THz absorption coefficient of PDMS as low as possible. As shown in bottom scale of Fig. 4(a), when the weighting percentage of PDMS decreased from 66.6% to the 50% (weight ratio of PDMS and Ag NPs decreased from 2:1 to 1:1), the transmission loss shows slight reduction from  $\sim 0.34$  to  $\sim 0.23$  dB/cm. The reason is ascribed to a larger covered region of the reflection layer by Ag

NPs, which increase the reflectivity of inner surface of the terahertz waveguides [49]. However, the loss dramatically increased when the weighting percentage of PDMS decreased from 50% to 33.3% (weight ratio of PDMS and Ag NPs increased from 1:1 to 1:2). This is due to a larger amount of Ag NPs in PDMS resulted in mixing difficulty [50] and a larger Ag NPs cluster was generated on the surface of coating layer, which increased the surface roughness and led to extra scattering losses. Therefore, 1:1 weight ratio of PDMS and Ag NPs was employed in this study.

As shown in Fig. 4(b), the measured losses of four flexible terahertz waveguides with 10 cm, 20 cm length and 2 mm, 4 mm bore diameters, respectively, were investigated as a function of THz QCL biased current. The losses of the 2 and 4 mm-bore diameter waveguides at  $\sim 2.58$  THz were almost stable when increasing the biased current from the threshold to peak bias condition of THz QCLs, corresponding to  $\sim 0.46$  dB/cm and  $\sim 0.22$  dB/cm, respectively and decreased when increasing the bore diameter. An ideal relationship between transmission loss ( $\alpha_t$ ) and bore diameter (D) is:

$$\alpha_t = \left( \frac{\mu_{lm}}{2\pi} \right)^2 \frac{8\lambda^2}{D^3} \text{Re}(v_l) \quad (1)$$

where  $\lambda$  is the incident wavelength in vacuum, D is the bore diameter,  $\mu_{lm}$  is the mode parameter of the  $lm^{\text{th}}$  mode, equal to the zeros of the Bessel function, l and m parameter is the number of periods or maximums and minimums in the azimuthal and radial direction, respectively. And  $\text{Re}(v_l)$  is a term which considers the mode supported, the refractive index of the reflective layer, and the geometry of the waveguide [51]. The ideal transmission loss is inversely proportional to the bore diameter cube of the waveguide, inside which the sidewall is perfectly smooth without any surface roughness at a given wavelength, thus no extra scattering loss. Furthermore, to investigate the relationship of transmission loss and length of waveguide, the transmission losses were characterized with 10 and 20 cm-length waveguides, respectively. For the waveguides with both 2 and 4 mm-bore diameters (photographs are shown in Fig. 4(c)), the transmission losses almost overlap with each other when the length of waveguide increased from 10 cm to 20 cm, indicating a preminent uniformity of the composite coating layer in the fabricated terahertz transmission waveguides.

The output beam profiles from the 3D-printed terahertz transmission waveguides with 2 mm and 4 mm-bore diameter and 20-cm length were recorded by a room-temperature terahertz camera (Uncooled FPA micro-bolometer array, Swiss Terahertz Rigi Series), allowing a real-time detection of spatial intensity distribution under different biases from threshold to peak bias condition of THz QCLs, as shown in Fig. 5. The waveguide with a 2 mm-bore diameter produced a single-mode Gaussian-like beam profile at the bias current of 3.38 A, 3.69 A, 3.74 A, 3.96 A and 4.03 A. A primary single-mode with a very tiny side lobe was observed in the output beam profiles from the waveguide with a 4 mm-bore diameter at the same bias current because a larger bore diameter is more likely to excite the higher order mode.

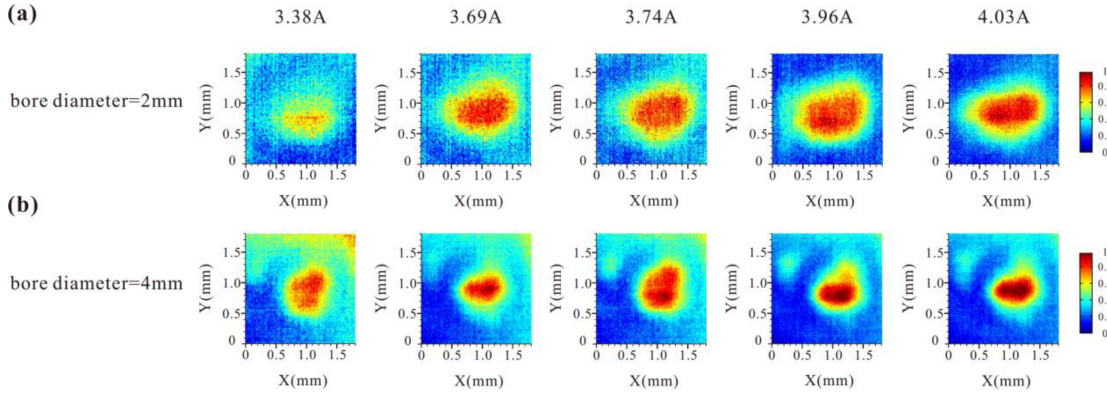


Fig. 5. Beam profiles of the output mode from terahertz transmission waveguides with (a) 2 mm and (b) 4 mm bore diameter when THz QCL is under different biases from threshold to peak condition.

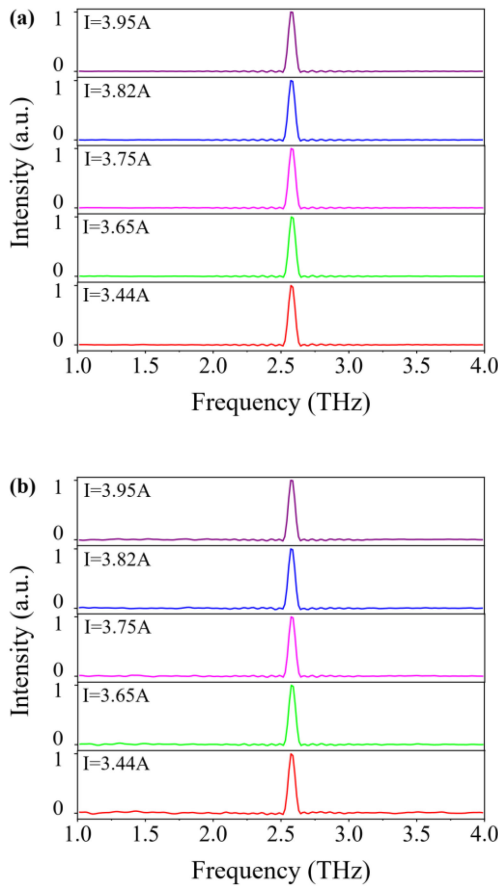


Fig. 6. Transmission spectra of the 3D-printed terahertz waveguides with (a) 4 mm and (b) 2 mm bore diameter under different biases.

To further investigate the transmission effect of the 3D-printed terahertz waveguides on the characteristics of output mode, transmission spectrum of the waveguides from threshold to peak bias of THz QCLs were measured by FTIR, as shown in the Fig. 6(a) and (b). The bias is 3.44A, 3.65A, 3.75A, 3.82A and 3.95A, respectively. The single-mode spectra of the THz QCLs are preserved after transmitting the 3D-printed terahertz waveguides with both two bore diameters 4 mm and 2 mm and no other spectral modes are excited during the transmission process [52].

Mechanical characteristics of being flexible, bendable, stretchable, stable and reliable are crucial for terahertz waveguides in various applications, such as in terahertz endoscopy or probe system. Additional loss will be introduced due to bending of waveguides [53]. To experimentally measure the bending loss of the 3D-printed flexible terahertz transmission waveguides, the input end of the 20 cm length waveguide was fixed and aligned to the spot focused by the lens, as seen in Fig. 2. The bending radius is 5 cm and Fig. 7(a) shows the total loss of waveguides with two bore diameters 2 mm and 4 mm measured at the bending angles of  $30^\circ$ ,  $45^\circ$  and  $60^\circ$ , respectively. For the waveguide with a 4 mm-bore diameter, total loss is  $\sim 5.6$  dB at a bending angle of  $60^\circ$  and  $\sim 3.3$  dB at a bending angle of  $30^\circ$ . In case of the waveguide with a 2 mm-bore diameter, total loss is  $\sim 8.8$  dB at a bending angle of  $60^\circ$  and  $\sim 4.9$  dB at a bending angle of  $30^\circ$ .

So far, there is few reports on the evaluations of antifatigue for flexible terahertz waveguides. As shown in the Fig. 7(b), the transmission losses of the fabricated flexible waveguides after multiple times of bending, up to 300 times were measured to investigate the mechanical endurance. The losses were nearly unchanged, which exhibit a superior mechanical endurance of the 3D-printed flexible terahertz transmission waveguide in this work owing to the high elastic coefficient of PDMS and fabricated materials of substrate tube. What's more, uniaxial tensile testing was carried out to the 3D-printed flexible terahertz waveguides. Due to the limitation of space in the mechanical force-strain testing instrument (TA Electroforce 3200), two 2-cm-long segments from the 10-cm-long waveguides with 2 mm and 4 mm-bore diameters were cut to verify the stretchability of the 3D-printed flexible terahertz waveguides. As shown in Fig. 7(c), there is a quasi-linear relationship between the strain of waveguides and tensile force. The strain  $\varepsilon$  was calculated according to the following formula [54]:

$$\varepsilon = \frac{l - l_0}{l} \times 100\% \quad (2)$$

where the  $l_0$  and  $l$  represent the lengths of testing waveguides prior to and after applying the loading force, respectively. Strain for the waveguides with two bore diameters is able to reach 40% by fully using the entire instrumental space. And the corresponding tensile force for 2 mm and 4 mm-bore diameter sample is

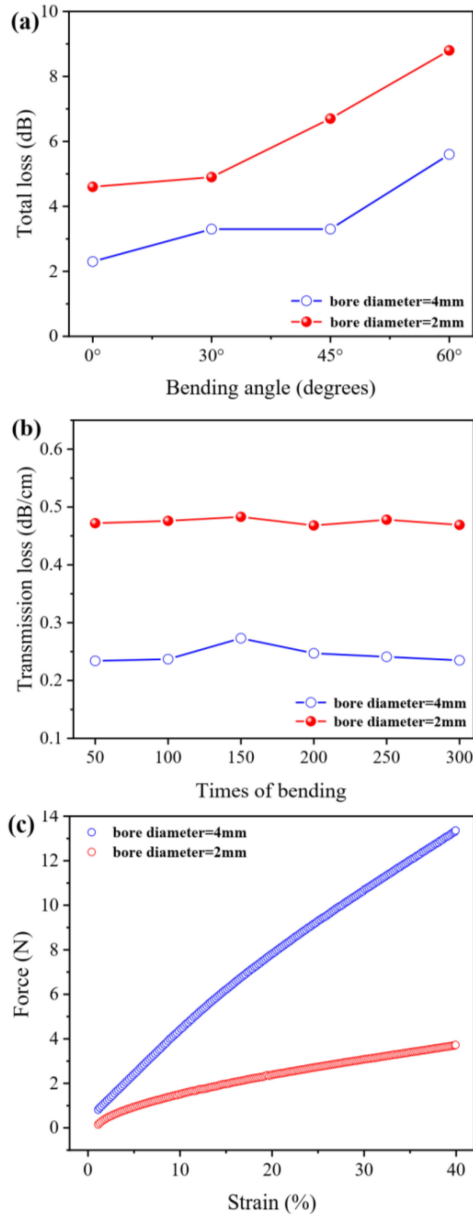


Fig. 7. (a) Total loss measured from the ratio between the output and input power of the 3D-printed flexible terahertz waveguides under different bending angles. (b) Transmission loss of the 3D-printed flexible terahertz waveguides under 50, 100, 150, 200, 250, and 300 times of bending, respectively. (c) Force-strain curves of the 3D-printed flexible terahertz waveguides with two bore diameters 2mm and 4mm.

$\sim 3.2\text{N}$  and  $\sim 13.7\text{N}$ , respectively. Thus, the 3D-printed flexible terahertz waveguides can be easily bent for a multitude of cycles owing to the excellent ductility. This work also reveals the potential applications of the 3D-printed terahertz waveguides in the ultra-flexible and stretchable terahertz devices.

#### IV. CONCLUSION

In summary, we demonstrated a novel flexible and stretchable terahertz transmission waveguide fabricated by 3D printing technology. The propagation characteristics of 2 mm and 4 mm-bore diameter waveguides were investigated at the frequency of 2.58

THz, which is the lasing frequency from the source of THz QCLs. The results show that the transmission losses are  $\sim 0.22$  dB/cm for the waveguides with a 4 mm-bore diameter. The roughness caused by the printing with accuracy ( $\pm 0.001$  to  $0.002$  inch per inch of part dimension) degrades the loss performance. Lower loss can be achieved by optimizing the composite ratio of PDMS and Ag NPs and further improving the inner surface smoothness of the 3D-printed waveguides. Single-mode output beam profiles from the 3D-printed waveguides under different bias conditions of THz QCLs were presented. Importantly, pre-eminent mechanical stability, reliability and flexibility of the 3D-printed terahertz transmission waveguides were tested and verified when bending up to more than 300 times. This work indicates that the low-cost, flexible 3D printing technology is able to provide an efficient way to design and fabricate high performance terahertz transmission waveguides, which will lead to broad applications in terahertz endoscopic and spectroscopic systems.

#### REFERENCES

- [1] M. Tonouchi, "Cutting-edge terahertz technology," *Nature Photon.*, vol. 1, no. 2, pp. 97–105, Feb. 2007.
- [2] X. Yang *et al.*, "Biomedical applications of terahertz spectroscopy and imaging," *Trends Biotechnol.*, vol. 34, no. 10, pp. 810–824, Oct. 2016.
- [3] S. T. Fan, Y. Z. He, B. S. Ung, and E. P.-. MacPherson, "The growth of biomedical terahertz research," *J. Phys. D: Apply. Phys.*, vol. 47, no. 374009, pp. 1–11, Aug. 2014.
- [4] W. Wang, F. P. Yan, S. Y. Tan, H. Zhou, and Y. F. Hou, "Ultrasensitive terahertz metamaterial sensor based on vertical split ring resonators," *Photon. Res.*, vol. 5, no. 6, pp. 571–577, Oct. 2017.
- [5] L. Zhao, S. Khanal, C. Z. Wu, and S. Kumar, "Proposal for a broadband THz refractive-index sensor based on quantum-cascade laser arrays," *Opt. Exp.*, vol. 23, no. 4, pp. 4751–4765, Feb. 2015.
- [6] L. A. Sterczewski *et al.*, "Terahertz hyperspectral imaging with dual chip-scale combs," *Optica.*, vol. 6, no. 6, pp. 766–771, Jun. 2019.
- [7] Y. Q. Cao *et al.*, "Characterization and discrimination of human colorectal cancer cells using terahertz spectroscopy," *Spectrochim. Acta. A.*, vol. 256, no. 119713, pp. 1–7, Mar. 2021.
- [8] S. Atakaramians, S. Afshar, T. M. Monro, and D. Abbott, "Terahertz dielectric waveguides," *Adv. Opt. Adv.*, vol. 5, no. 2, pp. 169–215, Jun. 2013.
- [9] M. S. Islam, C. M. B. Cordeiro, M. A. R. Franco, J. Sultana, A. L. S. Cruz, and D. Abbott, "Terahertz optical fibers," *Opt. Exp.*, vol. 28, no. 11, pp. 16089–16117, May 2020.
- [10] R. W. McGowan, G. Gallot, and D. Grischkowsky, "Propagation of ultrawideband short pulses of terahertz radiation through submillimeter-diameter circular waveguides," *Opt. Lett.*, vol. 24, no. 20, pp. 1431–1433, Oct. 1999.
- [11] M. Mbonye, R. Mendis, and D. M. Mittleman, "A terahertz two-wire waveguide with low bending loss," *Appl. Phys. Lett.*, vol. 95, no. 23, pp. 1–3, Dec. 2009.
- [12] R. Mendis and D. Grischkowsky, "Undistorted guided-wave propagation of subpicosecond terahertz pulses," *Opt. Lett.*, vol. 26, no. 11, pp. 846–848, Jun. 2001.
- [13] A. Mazhorova *et al.*, "Label-free bacteria detection using evanescent mode of a suspended core terahertz fiber," *Opt. Exp.*, vol. 20, no. 5, pp. 5344–5355, Feb. 2012.
- [14] T. Ma, H. Guerboukha, M. Girard, A. D. Squires, R. A. Lewis, and M. Skorobogatiy, "3D printed hollow-core terahertz optical waveguides with hyperuniform disordered dielectric reflectors," *Adv. Opt. Mater.*, vol. 4, no. 12, pp. 2085–2094, Sep. 2016.
- [15] X. L. Tang *et al.*, "Elliptical metallic hollow fiber inner-coated with non-uniform dielectric layer," *Opt. Exp.*, vol. 23, no. 17, pp. 22587–22601, Aug. 2015.
- [16] W. Talataisong *et al.*, "Hollow-core antiresonant terahertz fiber-based TOPAS extruded from a 3D printer using a metal 3D printed nozzle," *Photon. Res.*, vol. 9, no. 8, pp. 1513–1521, Jul. 2021.
- [17] B. S. Williams, "Terahertz quantum-cascade lasers," *Nature Photon.*, vol. 1, no. 10, pp. 517–525, Sep. 2007.

- [18] S. Kumar, B. S. Williams, Q. Qi, A. W. Lee, Q. Hu, and J. L. Reno, "Surface-emitting distributed feedback terahertz quantum-cascade lasers in metal-metal waveguides," *Opt. Exp.*, vol. 15, no. 1, pp. 113–128, Jan. 2007.
- [19] C. Z. Wu, S. Khanal, J. L. Reno, and S. Kumar, "Terahertz plasmonic laser radiating in an ultra-narrow beam," *Optica*, vol. 3, no. 7, pp. 734–740, Jul. 2016.
- [20] M. I. Amanti, G. Scalari, F. Castellano, M. Beck, and J. Faist, "Low divergence terahertz photonic-wire laser," *Opt. Exp.*, vol. 18, no. 6, pp. 6390–6395, Mar. 2010.
- [21] Y. Halioua *et al.*, "THz quantum cascade lasers operating on the radiative modes of a 2D photonic crystal," *Opt. Lett.*, vol. 39, no. 13, pp. 3962–3965, Jul. 2014.
- [22] C. Z. Wu, Y. Jin, J. L. Reno, and S. Kumar, "Large static tuning of narrow-beam terahertz plasmonic lasers operating at 78 K," *APL Photon.*, vol. 2, no. 2, pp. 1–9, Dec. 2017.
- [23] C. A. Curwen, J. L. Reno, and B. S. Williams, "Broadband continuous single-mode tuning of a short-cavity quantum-cascade VECSEL," *Nature Photon.*, vol. 13, pp. 855–859, Sep. 2019.
- [24] A. Khalatpour, A. K. Paulsen, C. Deimert, Z. R. Wasilewski, and Q. Hu, "High-power portable terahertz laser systems," *Nature Photon.*, vol. 15, pp. 16–20, Nov. 2020.
- [25] Y. Jin, J. L. Reno, and S. Kumar, "Phase-locked terahertz plasmonic laser array with 2 w output power in a single spectral mode," *Optica*, vol. 7, no. 6, pp. 708–715, Jun. 2020.
- [26] G. Xu *et al.*, "Efficient power extraction in surface-emitting semiconductor lasers using graded photonic heterostructures," *Nature Commun.*, vol. 3, no. 9522, pp. 1–7, Jul. 2012.
- [27] P. Tang, X. Chi, B. Chen, and C. Z. Wu, "Predictions of resonant mode characteristics for terahertz quantum cascade lasers with distributed feedback utilizing machine learning," *Opt. Exp.*, vol. 29, no. 10, pp. 15309–15326, May 2021.
- [28] Y. Jin, L. Gao, J. Chen, C. Z. Wu, J. L. Reno, and S. Kumar, "High power surface emitting terahertz laser with hybrid second- and fourth-order bragg gratings," *Nature Commun.*, vol. 9, no. 1911, pp. 1–7, Apr. 2018.
- [29] M. S. Vitiello *et al.*, "Guiding a terahertz quantum cascade laser into a flexible silver-coated waveguide," *J. Appl. Phys.*, vol. 110, no. 063312, pp. 1–5, Sep. 2011.
- [30] M. S. Vitiello *et al.*, "High efficiency coupling of terahertz micro-ring quantum cascade lasers to the low-loss optical modes of hollow metallic waveguides," *Opt. Exp.*, vol. 19, no. 2, pp. 1122–1130, Jan. 2011.
- [31] U. S. D. Cumis, J. -H. Xu, C. M. Bledt, J. A. Harrington, A. Tredicucci, and M. S. Vitiello, "2012-flexible, low-loss waveguide designs for efficient coupling to quantum cascade lasers in the far-infrared," *J. Infrared. Mil. Tera.*, vol. 33, no. 2, pp. 319–326, Feb. 2012.
- [32] R. De Gl'Innocenti *et al.*, "Hollow metallic waveguides integrated with terahertz quantum cascade lasers," *Opt. Exp.*, vol. 22, no. 20, pp. 24439–24449, Sep. 2014.
- [33] R. Wallis *et al.*, "Investigation of hollow cylindrical metal terahertz waveguides suitable for cryogenic environments," *Opt. Exp.*, vol. 24, no. 26, pp. 30002–30014, Dec. 2016.
- [34] R. Wallis *et al.*, "Efficient coupling of double-metal terahertz quantum cascade lasers to flexible dielectric-lined hollow metallic waveguide," *Opt. Exp.*, vol. 23, no. 20, pp. 26276–26287, Sep. 2015.
- [35] M. Nazarov *et al.*, "A flexible terahertz waveguide for delivery and filtering of quantum-cascade laser radiation," *Appl. Phys. Lett.*, vol. 113, no. 131107, pp. 1–3, Sep. 2018.
- [36] A. L. S. Cruz, C. M. B. Cordeiro, and M. A. R. Franco, "3D printed hollow-core terahertz fibers," *Fibers*, vol. 6, no. 3, pp. 1–11, Jun. 2018.
- [37] W. J. Otter *et al.*, "3D printed 1.1 THz waveguides," *Electron. Lett.*, vol. 53, no. 7, pp. 471–473, Oct. 2017.
- [38] J. Yang *et al.*, "3D printed low-loss THz waveguide based on Kagome photonic crystal structure," *Opt. Exp.*, vol. 24, no. 20, pp. 22454–22460, Oct. 2016.
- [39] S. Pandey, B. Gupta, and A. Nahata, "Terahertz plasmonic waveguides created via 3D printing," *Opt. Exp.*, vol. 21, no. 21, pp. 24422–24430, Oct. 2013.
- [40] J. W. Li, K. Nallappan, H. Guerboukha, and M. Skorobogatiy, "3D printed hollow core terahertz Bragg waveguides with defect layers for surface sensing applications," *Opt. Exp.*, vol. 25, no. 4, pp. 4126–4144, Feb. 2017.
- [41] D. W. Vogt and R. Leonhardt, "3D-printed broadband dielectric tube terahertz waveguide with anti-reflection structure," *J. Infrared. Milli. Terahz. Waves*, vol. 37, pp. 1086–1095, Jun. 2016.
- [42] M. Asensio, V. Costa, A. Nohales, O. Bianchi, and C. Gómez, "Tunable structure and properties of segmented thermoplastic polyurethanes as a function of flexible segment," *Polymers*, vol. 11, no. 12, pp. 1–19, Nov. 2019.
- [43] S. Alfihed, J. F. Holzman, and I. G. Foulds, "Developments in the integration and application of terahertz spectroscopy," *Biosens. Bioelectron.*, vol. 165, no. 112393, pp. 1–11, Jun. 2020.
- [44] K. Zhang, H. Wang, K. Yao, G. He, Z. Zhou, and D. Sun, "Surface roughness improvement of 3D printed microchannel," *J. Micromech. Microeng.*, vol. 30, no. 065003, pp. 1–10, Apr. 2020.
- [45] S. Alfihed, M. H. Bergen, J. F. Holzman, and I. G. Foulds, "A detailed investigation on the terahertz absorption characteristics of polydimethylsiloxane (PDMS)," *Polymer*, vol. 153, pp. 325–330, Jun. 2018.
- [46] H. Zhu *et al.*, "Terahertz master-oscillator power-amplifier quantum cascade lasers," *Appl. Phys. Lett.*, vol. 109, no. 231105, pp. 1–5, Dec. 2016.
- [47] H. M. Soe, A. A. Manaf, A. Matsuda, and M. Jaafar, "Development and fabrication of highly flexible, stretchable, and sensitive strain sensor for long durability based on silver nanoparticles-polydimethylsiloxane composite," *J. Mater. Sci. Mater. Electron.*, vol. 31, pp. 11897–11910, Jun. 2020.
- [48] B. Bowden, J. A. Harrington, and O. Mitrofanov, "Silver/polystyrene-coated hollow glass waveguides for the transmission of terahertz radiation," *Opt. Lett.*, vol. 32, no. 20, pp. 2945–2947, Oct. 2007.
- [49] L. M. Li and W. S. Chin, "Rapid fabrication of flexible and transparent Ag Nanocubes@PDMS film as SERS substrate with high performance," *ACS Appl. Mater. Inter.*, vol. 12, pp. 37538–37548, Jul. 2020.
- [50] S. M. Mehdi, K. H. Cho, and K. H. Choi, "Stretchability and resistive behavior of silver (Ag) nanoparticle films on polydimethylsiloxane (PDMS) with random micro ridges," *J. Mater. Sci. Mater. El.*, vol. 25, pp. 3375–3382, Jun. 2014.
- [51] J. A. Harrington, *Infrared Fibre Optics and Their Applications*. Bellingham, WA, USA: SPIE, 2004, pp. 1–293.
- [52] B. Gerislioglu, A. Ahmadvand, and N. Pala, "Single- and multimode beam propagation through an optothermally controllable fano clusters-mediated waveguide," *J. Lightw. Technol.*, vol. 35, no. 22, pp. 4961–4966, Nov. 2017.
- [53] T. Ito, Y. Matsuura, M. Miyagi, H. Minamide, and H. Ito, "Flexible terahertz fiber optics with low bend-induced losses," *J. Opt. Soc. Amer. B.*, vol. 24, no. 5, pp. 1230–1235, May. 2007.
- [54] L. Zhang, H. Q. Li, X. J. Lai, T. Y. Gao, and X. R. Zeng, "Three-dimensional binary-conductive-network silver nanowires@Thiolated graphene foam-based room-temperature self-healable strain sensor for human motion detection," *ACS Appl. Mater. Inter.*, vol. 12, pp. 44360–44370, Jul. 2020.